# A NUMERICAL STUDY OF COSSERAT BEAM THEORY APPLIED TO THE MODELING OF SUBSEA RISERS

**Adailton Silva Borges, asborges@mecanica.ufu.br**
**Wellington Luziano Paulo Júnior, wellingtonlpaulo@gmail.com**
**Domingos Alves Rade, domingos@ufu.br**
**Aristeu da Silveira Neto, aristeus@mecanica.ufu.br**
Federal University of Uberlândia, Avenida João Naves de Ávila, 2121. Bairro Santa Mônica, Uberlândia, MG.

***Abstract.*** *This work presents a methodology for the modeling of flexible slender beamlike structures, with application the submarine risers used for oil extraction. Due to the typically large aspect ratio, the behavior of these structures can be better represented in the context of large-displacement nonlinear theories, among which Cosserat beam theory has been chosen in the study reported herein. In this theory, the configuration of the deformed beam is described through the vector displacement of the centroid curve, and an orthonormal moving frame, rigidly attached to the cross-section of the beam. The orientation of the moving frame, relative to the inertial one, is parameterized using three consecutive elementary rotations. To main advantage of this theory it is in the fact that the form functions are obtained by static equilibrium equations and, as a result, geometric nonlinearities of the system are fully taken into account. To account for the excitations exerted by the surrounding fluid, a one-way approach is adopted in which the hydrodynamic forces are provided by semi-empirical expressions. The theoretical foundations are fist reviewed, followed by numerical simulations that put in evidence the main features of the modeling methodology.*

***Keywords****: Cosserat beam theory, structural dynamics, offshore structures, finite elements,*

## 1. INTRODUCTION

In the context of the offshore industry, flexible risers are shallow structural components designed with the purpose of transporting the pressured oil from the well to the platform. Their design involves technological challenges as they are becoming increasingly longer as the result of deeper oil exploitation. Also, during their operation they are subjected to very complex scenarios resulting from the combination of static and dynamic loads such as: internal pressure, self-weight, residual stress resulting from the installation procedure and vibrations induced by water motion (vortex-induced vibrations-VIV) and the vertical motion of the platform. Thus, the safe and cost-effective design of such structures requires a deep understanding of their mechanical behavior, which can be gained by the use of numerical models capable of accounting for the actual geometry and load conditions, especially fluid-structure interaction.

Pesce (1997) discusses the behavior of long risers, stating that it can be better represented by the theory of flexible lines than the classical beam theory, owing to their slender profile. In this context, the author refers to the Cosserat beam theory. This nonlinear theory was developed in the XVIIth century by the Cosserat brothers, and has been revisited and applied to engineering problems in the last few years, as the increase of computer power enables dealing with highly nonlinear differential equations.

As opposed to traditional Euler-Bernoulli or Timoshenko beam theories, the Cosserat beam theory geometrically exact, in the sense that it is not based on geometric approximations. In this theory, the deformed configuration of the beam is described by the displacement vector of the centroid curve and an orthonormal moving frame, rigidly attached to the cross section of the beam. The orientation of the orthonormal moving frame, with respect to an inertial system, is parameterized using three consecutive elementary rotations. Thus, the equations of motion are nonlinear differential equations in terms of time and space variables. For static problems, the equilibrium equations become nonlinear ordinary differential equations in terms of a space variable, which can be approximately solved by using standard techniques as the perturbation.

Aiming at solving the nonlinear equations of motion, Simo (1985) and Vu-Quoc (1986) combined the finite element theory to the formulation. In this condition, the displacement functions of the beam are obtained as a function of the nodal displacements and rotations. The main advantage of this procedure is related to the fact that the shape functions are obtained from differential equations of motion, and therefore take into account all the nonlinearities of the system. Consequently, one can ensure satisfactory accuracy of response predictions by dividing the structure in a number of elements which is significantly smaller than the number required by finite element discretization based on low order polynomial shape functions.

Recent publications like Alamo (2006) used that methodology, from the second order shape function, to model slender structures, with applications in oil drilling columns. And Santos (2007) uses the methodology, but instead uses adopted shape functions, low order polynomial to modeling submerged cables from an initial configuration of equilibrium and excited by the movement of the platform and by the flow of sea water obtained empirically using the Morison's equations.

In this paper the main characteristics of the Cosserat theory are first reviewed. The numerical implementation of the modeling theory is validated and assessed through comparison with the data obtained from the literature. Finally, a cylinder that resembles a real flexible riser used in oil industry is modeled, aiming at characterizing the motion under the action of surrounding flow. In this first simulation, the forces applied by the fluid are obtained from empirical Morison equations of for submerged cables. This procedure will be used to provide support for future implementations, in which the fluid will be modeled using full 3D computational fluid dynamics.

## 2. THEORETICAL FRAMEWORK

According to the Cosserat theory, the behavior of a slender beam is modeled in terms of the motion in space by the line passing through the centroids of the cross sections, defined by the vector **r**(s) in a Cartesian fixed (inertial) base {$\mathbf{e}_1$, $\mathbf{e}_2$, $\mathbf{e}_3$} and a set of orthogonal unit vectors attached to the cross section {$\mathbf{d}_1$(s), $\mathbf{d}_2$(s), $\mathbf{d}_3$(s)}. In Figure 1 it can be seen that $\mathbf{d}_1$(s) and $\mathbf{d}_2$(s) are contained in the cross section plane whilst $\mathbf{d}_3$(s) is perpendicular to that plane. In summary, the elementary configuration in the beam theory of Cosserat is described by a line of centroids **r**(s) and three orthogonal unit vectors.

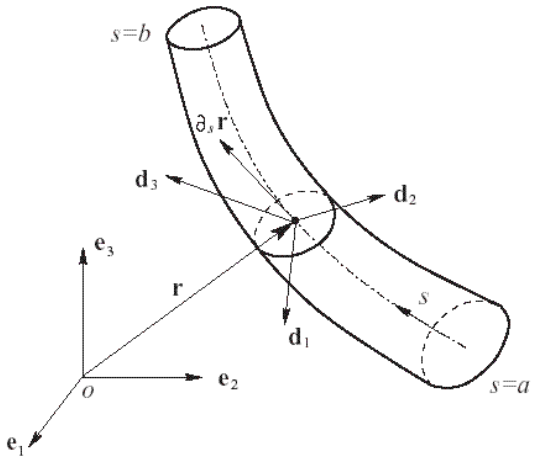


Figure 1. Schematic model of an element of Cosserat.

The beam theory of Cosserat classifies the strain into two groups: linear strain **v**(s) and angular strain **u**(s). The components $\mathbf{v}_1$(s) and $\mathbf{v}_2$(s) are called shear strain and $\mathbf{v}_3$(s) is named elongation. While $\mathbf{u}_1$(s) and $\mathbf{u}_2$(s) are described as bending strain, $\mathbf{u}_3$(s) is called the torsion strain.

The linear strain vector **v**(s) is obtained by the derivation of the position of the centroidal point along the coordinate s, as given by Eq. (1).

$$^F\mathbf{v}(s) = \frac{d\,^F\mathbf{r}(s)}{ds} = \left|r'(s)\right| {}^F\mathbf{d}_3(s) \tag{1}$$

The angular strain vector **u**(s) is obtained from the derivative in the space of the mobile base $\mathbf{d}_i$(s), according to Eq. (2).

$$\frac{d\,\mathbf{d}_i(s)}{ds} = \mathbf{u}(s,t) \times \mathbf{d}_i(s,t) \tag{2}$$

To describe the relationship between the orthonormal moving frame and the fixed base two methods of parameterization can be employed: the Euler vector or three elementary rotations (Euler's angles). The transformation matrices found for the Euler's vector method and the Euler's angles method are presented in the Eq. (3) and Eq. (4), respectively.

$$F_{\mathbf{T}}{}^{S} = \begin{bmatrix} \dfrac{(v_2^2 + v_3 v_1^2)\cos\varphi}{v_1^2 + v_2^2} + \dfrac{(v_3 - 1)v_1 v_2 \sin\varphi}{v_1^2 + v_2^2} & \dfrac{(v_3 - 1)v_1 v_2 \cos\varphi}{v_1^2 + v_2^2} - \dfrac{(v_2^2 + v_3 v_1^2)\sin\varphi}{v_1^2 + v_2^2} & v_1 \\ \dfrac{(v_3 - 1)v_1 v_2 \cos\varphi}{v_1^2 + v_2^2} + \dfrac{(v_1^2 + v_3 v_2^2)\sin\varphi}{v_1^2 + v_2^2} & \dfrac{(v_1^2 + v_3 v_2^2)\cos\varphi}{v_1^2 + v_2^2} - \dfrac{(v_3 - 1)v_1 v_2 \sin\varphi}{v_1^2 + v_2^2} & v_2 \\ -v_1\cos\varphi - v_2\sin\varphi & v_1\sin\varphi - v_2\cos\varphi & v_3 \end{bmatrix} \tag{3}$$

$$F_{\mathbf{T}}{}^{S} = \begin{bmatrix} \cos\phi_z\cos\phi_y & -\sin\phi_z\cos\phi_y & \sin\phi_y \\ \sin\phi_x\sin\phi_y\cos\phi_z + \cos\phi_x\sin\phi_z & \cos\phi_x\cos\phi_z - \sin\phi_x\sin\phi_y\sin\phi_z & -\sin\phi_z\cos\phi_y \\ \sin\phi_x\sin\phi_z - \cos\phi_x\sin\phi_y\cos\phi_z & \cos\phi_x\sin\phi_y\sin\phi_z + \sin\phi_x\cos\phi_z & \cos\phi_z\cos\phi_y \end{bmatrix} \tag{4}$$

Note that the angle $\varphi$ measures the torsion of the beam along the coordinate s, and $\phi_x$, $\phi_y$, $\phi_z$ are respectively the rotations around the axes x, y and z.

Introducing polynomial expansions of the trigonometric functions appearing in Eq. (4) and matching the resulting expressions to those of Eq. (3), algebraic equations are obtained, which can be mathematically manipulated and truncated up to the third order to obtain the relationships between $\{\varphi(s), x'(s), y'(s)\}$ and $\{\phi_x(s), \phi_y(s), \phi_z(s)\}$ as given in Eq. (5) and (6):

$$\begin{aligned} \varphi(s) &= \phi_z(s) + \frac{1}{2}\phi_x(s)\phi_y(s) - \frac{1}{6}\phi_z^3(s) \\ v_1 &= \frac{x'(s)}{r'(s)} = +\phi_y(s) - \frac{1}{6}\phi_y^3(s) \\ v_2 &= \frac{y'(s)}{r'(s)} = -\phi_x(s) + \frac{1}{2}\phi_x(s)\phi_y^2(s) + \frac{1}{6}\phi_x^3(s) \end{aligned} \tag{5}$$

$$\begin{aligned} \phi_x(s,t) &= -v_2(s,t) + \frac{1}{2}\varphi(s,t)v_1(s,t) - \frac{1}{6}(v_1^2(s,t) + v_2^2(s,t) - \frac{1}{2}\varphi^2(s,t))v_2(s,t) \\ \phi_y(s,t) &= v_1(s,t) + \frac{1}{2}\varphi(s,t)v_2(s,t) + \frac{1}{6}(v_1^2(s,t) + v_2^2(s,t) - \frac{1}{2}\varphi^2(s,t))v_1(s,t) \\ \phi_z(s,t) &= \varphi(s,t) - \frac{1}{12}(v_1^2(s,t) + v_2^2(s,t))\varphi(s,t) \end{aligned} \tag{6}$$

The local dynamic behavior of a beam element of Cosserat, as shown by Antman (1995), is given by partial differential equations given in Eq. (7), where ${}^{S}\mathbf{n}(s,t)$ is the contact force, ${}^{S}\mathbf{m}(s,t)$ is the resulting contact moment, ${}^{S}\mathbf{h}(s,t)$ is the angular momentum, ${}^{S}\mathbf{f}(s,t)$ is the external density force and ${}^{S}\mathbf{l}(s,t)$ is the external momentum density.

$$\begin{aligned} \rho(s)A(s)\frac{d^2\,{}^{S}\mathbf{r}(s,t)}{dt^2} &= \frac{d\,{}^{S}\mathbf{n}(s,t)}{ds} + {}^{S}\mathbf{f}(s,t) \\ \frac{d\,{}^{S}\mathbf{h}(s,t)}{dt} &= \frac{d\,{}^{S}\mathbf{m}(s,t)}{ds} + {}^{S}\tilde{\mathbf{v}}(s,t)\,{}^{S}\mathbf{n}(s,t) + {}^{S}\mathbf{l}(s,t) \end{aligned} \tag{7}$$

The displacement functions of the beam, expressed in terms of the nodal displacements and rotations are derived from the resolution of the static equilibrium equations. However, for static equilibrium, the equations of motion become ordinary differential equations, in the absence of external forces and gravity. After mathematical manipulations, the following equations are obtained:

$$\begin{aligned} n_1'(s) &= u_3(s)n_2(s) - u_2(s)n_3(s) \\ n_2'(s) &= u_1(s)n_3(s) - u_3(s)n_1(s) \\ n_3'(s) &= u_2(s)n_1(s) - u_1(s)n_2(s) \\ m_3'(s) &= u_2(s)m_1(s) - u_1(s)m_2(s) \end{aligned} \tag{8}$$

In Eq. (8) the term *n(s,t)* represents the contact force per unit length, *m(s,t)* is the contact moment (internal) resultant per unit length, *h(s,t)* is the angular momentum per unit length, *f(s,t)* is the external force density per unit length and *l(s,t)* is the external momentum density per unit length.

To find the shape functions it is necessary to solve the highly nonlinear system above, noting that it cannot be solved by direct integration. Therefore, the perturbation method is used to obtain the approximated solution (Nayfeh, 1985). The resolution of this system was performed using symbolic manipulation software. For details the reader should consult the paper by Cao (2005). To investigate deflection up to third order nonlinearity in the perturbation parameter ε, it is adequate to adopt the following truncated Eq.(9) to $\varepsilon^3$ order terms. Then, the general displacement components of the beam in the domain s = [0, L] are given by:

$$\begin{aligned} x(s) &= \varepsilon\, x_1(s) + \varepsilon^2 x_2(s) + \varepsilon^3 x_3(s) \\ y(s) &= \varepsilon\, y_1(s) + \varepsilon^2 y_2(s) + \varepsilon^3 y_3(s) \\ z(s) &= s + \varepsilon\, z_1(s) + \varepsilon^2 z_2(s) + \varepsilon^3 z_3(s) \\ \varphi(s) &= \varepsilon\, \varphi_1(s) + \varepsilon^2 \varphi_2(s) + \varepsilon^3 \varphi_3(s) \end{aligned} \tag{9}$$

The dynamic equations of motion are obtained by using the extended Hamilton Principle, which is given by Eq. (10) where, *T* is the total kinetic energy of the system, *V* is the potential energy associated with the conservative forces and $\delta W_{NC}^F$ is the virtual work of the non conservative forces.

$$\delta \int_{t_1}^{t_2} (T - V)dt + \int_{t_1}^{t_2} \delta W_{NC}^F dt = 0 \tag{10}$$

Therefore it is necessary to derive the expressions of the kinetic and potential energies of the Cosserat beam. In Fig. 1 it is possible to see that the motion of the beam involves two velocities, one is the translation of the centroid curve and the other is the angular velocity of the cross section. The kinetic energy per unit length is given by Eq. (11), where **M**(s) is the mass matrix, depending on the s position of the centroid line, **I**(s) is the matrix of inertia, depending on the s position of the centroid line and ${}^S\mathbf{w}(s,t)$ is the angular velocity of the cross section.

$$T = \frac{1}{2}\frac{d}{dt}({}^F\mathbf{r}(s,t))M(s)\frac{d}{dt}({}^F\mathbf{r}(s,t)) + \frac{1}{2}{}^S\mathbf{w}^T(s,t){}^S I\, {}^S\mathbf{w}(s,t) \tag{11}$$

On other hand, considering small strains, the elastic potential energy, per unit length, can be expressed in terms of the strain vectors $\mathbf{v}(s,t)$ and $\mathbf{u}(s,t)$, as given by Eq. (12):

$$U = \frac{1}{2}{}^S\mathbf{v}^T(s,t)\mathbf{K}(s){}^S\mathbf{v}(s,t) + \frac{1}{2}{}^S\mathbf{u}^T(s,t)\mathbf{J}(s){}^S\mathbf{u}(s,t) \tag{12}$$

Since **K(s)** and **J(s)** are given by constitutive relations that will not be shown in this paper for convenience, for more information the interested reader is advised to refer to (Cao, 2005). It is convenient to rewrite the energy expressions as function of the dimensionless variables defined by Eq. (13), where $\omega_0$ is the natural frequency, to be determined later, $L_0$ is the size of the element.

$$\sigma = \frac{s}{L_0}, \bar{\mathbf{r}} = \frac{\mathbf{r}}{L_0}, \bar{x} = \frac{x}{L_0}, \bar{y} = \frac{y}{L_0}, \bar{z} = \frac{z}{L_0}, \tau = \omega_0 t, \tag{13}$$

The nodal displacement and the rotation can be expressed as a vector in function of a previously picked set of generic coordinates assuming that the dimensionless variation of displacement in the edges of the element ($\sigma = a / L_0$ and $\sigma = b / L_0$) is given by Eq. (14).

$$\mathbf{q}_a(\tau) = [x_a(\tau) \quad y_a(\tau) \quad z_a(\tau) \quad \phi_{xa} \quad \phi_{ya} \quad \phi_{za}]^T \tag{14}$$

And Eq. (15)

$$\mathbf{q}_b(\tau) = [x_b(\tau) \quad y_b(\tau) \quad z_b(\tau) \quad \phi_{xb} \quad \phi_{yb} \quad \phi_{zb}]^T \tag{15}$$

So, the generic vector of displacement for the element can be described by Eq. (16).

$$\mathbf{q}^e(\tau) = [q_a^T \quad q_b^T]^T \tag{16}$$

The generic degrees of freedom represented by the Eq. (14) and Eq. (15) can be seen in Figure 2, where a and b are the nodes in the edge of the element.

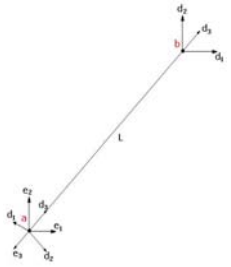

Figure 2. Cosserat beam element.

Rearranging Eq. (11) and making the necessary mathematical manipulations, it is possible to find the relationship given by Eq. (17), that refers to the kinetic energy of the beam, and using a similar manner it is possible to find the potential energy of the beam, given by Eq. (18).

$$T = \frac{1}{2}\left\{\rho A \omega_0^2 L_0 \dot{\bar{\mathbf{r}}} \cdot \dot{\bar{\mathbf{r}}} + \omega_0^2 (\bar{\mathbf{w}}, \bar{\mathbf{w}})\right\} \tag{17}$$

$$U = \frac{1}{2}\left\{\frac{1}{L_0^2}\mathbf{J}(\bar{\mathbf{u}}, \bar{\mathbf{u}}) + K_{33}(\bar{v}_3 - 1)^2\right\} \tag{18}$$

The temporal variations of displacements and rotations of a cross section inside the element can be expressed as combinations of the shape functions previously obtained, leading to a nonlinear functions of the dimensionless space variable $\sigma$ and of the nodal displacement vector $\mathbf{q}^e(\tau)$, as follows:

$$\bar{x} = \bar{x}(\sigma, \mathbf{q}^e(\tau)), \quad \bar{y} = \bar{y}(\sigma, \mathbf{q}^e(\tau))y, \quad \bar{z} = \bar{z}(\sigma, \mathbf{q}^e(\tau))z \quad \bar{\varphi} = \bar{\varphi}(\sigma, \mathbf{q}^e(\tau)) \tag{19}$$

or:

$$\bar{\mathbf{r}} = \bar{\mathbf{r}}(\sigma, \mathbf{q}^e(\tau)) \tag{20}$$

Making the necessary mathematical manipulations, the kinetic energy density and the potential energy density are given as follows:

$$T = T(\sigma, \mathbf{q}^e(\tau), \dot{\mathbf{q}}^e(\tau)), \quad U = U(\sigma, \mathbf{q}^e(\tau)) \tag{21}$$

That way it is possible to define the Lagrangian given by Eq. (22):

$$L(\mathbf{q}^e(\tau), \dot{\mathbf{q}}^e(\tau)) = T(\sigma, \mathbf{q}^e(\tau), \dot{\mathbf{q}}^e(\tau)) - U(\sigma, \mathbf{q}^e(\tau)) = \int_0^l \left[ T(\sigma, \mathbf{q}^e(\tau), \dot{\mathbf{q}}^e(\tau)) - U(\sigma, \mathbf{q}^e(\tau)) \right] L_0 d\sigma \tag{22}$$

The virtual work done by the non conservative forces, whose resultant is denoted by $\mathbf{F}^{NC}$ is expressed as:

$$\int_{t_1}^{t_2} \delta W_{nc}^F dt = \int_{t_1}^{t_2} \sum_{j=1}^{N} (F_i^{nc} \cdot \delta r_i) dt = \int_{t_1}^{t_2} \sum_{j=1}^{N} Q_j \delta q_j dt \tag{23}$$

where $Q_j$ are the generalized forces.

It is assumed that the forces that act on the element are composed of three additive parts. The first is from the interaction between neighboring elements, the second is due to the action of external forces concentrated in nodal points, and the third represents the external forces distributed with fixed directions and prescribed intensity. Therefore, the interaction of neighboring elements, in this work will be called internal forces and moments. The internal forces in the nodes at the edge of the element *a* (σ=0) and *b* (σ=L) are given by Eq. (24).

$$\mathbf{f}_a^i(\tau) = \begin{bmatrix} f_{ax}(\tau) & f_{ay}(\tau) & f_{az}(\tau) \end{bmatrix}^T, \quad \mathbf{f}_b^i(\tau) = \begin{bmatrix} f_{bx}(\tau) & f_{by}(\tau) & f_{bz}(\tau) \end{bmatrix}^T \tag{24}$$

The moments of internal interaction are given by:

$$\mathbf{l}_a^i(\tau) = \begin{bmatrix} l_{ax}(\tau) & l_{ay}(\tau) & l_{az}(\tau) \end{bmatrix}^T, \quad \mathbf{l}_b(\tau) = \begin{bmatrix} l_{bx}(\tau) & l_{by}(\tau) & l_{bz}(\tau) \end{bmatrix}^T \tag{25}$$

The concentrated forces and moments are expressed as follows:

$$\mathbf{f}_a^c(\tau) = \begin{bmatrix} f_{xa}^c & f_{ya}^c & f_{za}^c \end{bmatrix}^T, \quad \mathbf{f}_b^c(\tau) = \begin{bmatrix} f_{xb}^c & f_{yb}^c & f_{zb}^c \end{bmatrix}^T, \quad \mathbf{l}_a^c = \begin{bmatrix} l_{xa}^c & l_{ya}^c & l_{za}^c \end{bmatrix}, \quad \mathbf{l}_b^c = \begin{bmatrix} l_{xb}^c & l_{yb}^c & l_{zb}^c \end{bmatrix} \tag{26}$$

Finally, the distributed forces $(\xi_i)$ and the distributed moments $(\eta_i)$ are given by Eq. (27):

$$\boldsymbol{\xi}^d = \begin{bmatrix} \xi_x^d & \xi_y^d & \xi_z^d \end{bmatrix}, \quad \boldsymbol{\eta}^d = \begin{bmatrix} \eta_x^d & \eta_y^d & \eta_z^d \end{bmatrix} \tag{27}$$

The virtual work don by a distributed load (Cao, 2005) is given by:

$$\delta W^d = \int_0^l \left( \xi_x^d \delta\bar{x} + \xi_y^d \delta\bar{y} + \xi_z^d \delta\bar{z} + \eta_x^d \delta\varphi_x + \eta_y^d \delta\varphi_y + \eta_z^d \delta\varphi_z \right) L_0 d\sigma \tag{28}$$

Therefore, it is possible to write:

$$f^{de}(\tau, \mathbf{q}^e) = \left[ \begin{array}{l} \displaystyle\int_0^l \left( \xi_x^d \frac{\partial \bar{x}(\sigma, \mathbf{q}^e)}{\partial q^e} + \xi_y^d \frac{\partial \bar{y}(\sigma, \mathbf{q}^e)}{\partial q^e} + \xi_z^d \frac{\partial \bar{z}(\sigma, \mathbf{q}^e)}{\partial q^e} + \eta_x^d \frac{\partial \phi_x(\sigma, \mathbf{q}^e)}{\partial q^e} \right) + \\ \displaystyle\int_0^l \left( \eta_y^d \frac{\partial \phi_y(\sigma, \mathbf{q}^e)}{\partial q^e} + \eta_z^d \frac{\partial \phi_z(\sigma, \mathbf{q}^e)}{\partial q^e} \right) \end{array} \right] \delta q^e L_0 d\sigma \tag{29}$$

Rearranging the internal forces and internal moments in elementary terms, one writes:

$$\mathbf{f}^{ie}(\tau) = \begin{bmatrix} f_a^i(\tau) & l_a^i(\tau) & f_b^i(\tau) & l_b^i(\tau) \end{bmatrix} \tag{30}$$

The elementary external forces and moments are similarly given by:

$$\mathbf{f}^{ce}(\tau) = \begin{bmatrix} f_a^c(\tau) & l_a^c(\tau) & f_b^c(\tau) & l_b^c(\tau) \end{bmatrix} \tag{31}$$

Therefore, the virtual work done by the additive forces is expressed as follows:

$$\delta W_{NC}^F = \left(\mathbf{f}^{ie} + \mathbf{f}^{ce} + \mathbf{f}^{de}\right)^T \cdot \delta\mathbf{q}^e \tag{32}$$

Associating Eq. (22), Eq. (24) and Eq. (10), and using the chain rule and integration by parts, we have the Lagrange equation for the motion of a Cosserat element given by Eq. (33).

$$\frac{d}{d\tau}\left(\frac{\partial L}{\partial \dot{q}_j}\right) - \frac{\partial L}{\partial q_j} = \mathbf{f}_j^{ie} + \mathbf{f}_j^{ce} + \mathbf{f}_j^{de} \tag{33}$$

After several mathematical manipulations, we find the ordinary differential equation of motion with nonlinearities of the same order of the displacement functions (third order), represented by Eq. (34), where $\mathbf{M}_1^e$ and $\mathbf{M}_2^e$ are the mass matrices (both linear), $\mathbf{K}^e$ is the linear stiffness matrix and $\mathbf{g}^e(\mathbf{q}^e)$ is a nonlinear vector with quadratic an cubic terms on the components of $\mathbf{q}^e$. Then, $\mathbf{f}^{ie}(\tau)$ is the elementary internal force and momentum vector, $\mathbf{f}^{ce}(\tau)$ is the elementary external concentrated force and moment vector and $\mathbf{f}^{de}(\tau, \mathbf{q}^e)$ is the elementary distributed moment vector. The contour conditions, as well as the global equations of the systems are mounted using they are mounted the similar form the classic theory of finite elements. For more details of this implementation and the construction of global matrix of the system, see Cao (2005).

$$(\mathbf{M}_1^e + \mathbf{M}_2^e)\ddot{\mathbf{q}}^e + \mathbf{K}^e\mathbf{q}^e + \mathbf{g}^e(\mathbf{q}^e) = \mathbf{f}^{ie}(\tau) + \mathbf{f}^{ce}(\tau) + \mathbf{f}^{de}(\tau, \mathbf{q}^e) \tag{34}$$

For transient analysis of nonlinear structural problems it is necessary to use a stable and accurate method of time integration, especially when the solution is to be simulated in long time periods. Methods that prove to be stable in linear analysis could be the first choice for applications to nonlinear problems, but it has been verified that these methods do not remain stable when large displacements are involved and long periods of response simulations. This fact is directly linked to the inability of traditional methods to preserve the total energy and momentum of the system, which makes them numerically unstable (Bathe, 2007). The so-named composed method of time integration may be a viable alternative when the traditional methods such as Newmark's method become unsuitable.

The feature of stability over the integration time is crucial in fluid-structure simulations, as the simulation time is relatively long, especially when CFD methods are used to simulate the flow. Thus, to avoid this problem, we chose to implement the Bathe's composed method to integrate the global equations of the system, which were obtained from the elementary equations of the system using the Eq. (34); this method will be used in future fluid-structural implementations.

## 3. NUMERICAL APPLICATIONS

### 3.1. Modeling of a slender cantilever beam

First, to validate the implemented algorithm, we will simulate a structure found in the literature, and this confrontation will enable to evaluate the modeling methodology and the integration method used. The Figure 3 represents the simulated structure.

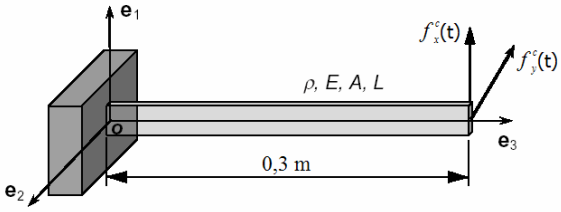


Figure 3. Model used to validate the methodology

This beamlike structure was first studied by Cao (2005), having a length of 0.3 meters and a rectangular cross section of constant width of 0.01 m and 0.005 m of thickness. The values adopted for the Young modulus and mass density are respectively 2.08e8 Pa and 3.0e3 kg/m³. The harmonic excitation forces in *x* and *y* directions are respectively $f_x^c(t) = 0.01\cos(8t)$ and $f_y^c(t) = 0.005\sin(8t)$. Figure 4 shows a comparison between the displacement time histories at the free end of the beam, which was discretized using 10 finite elements of equal lengths.

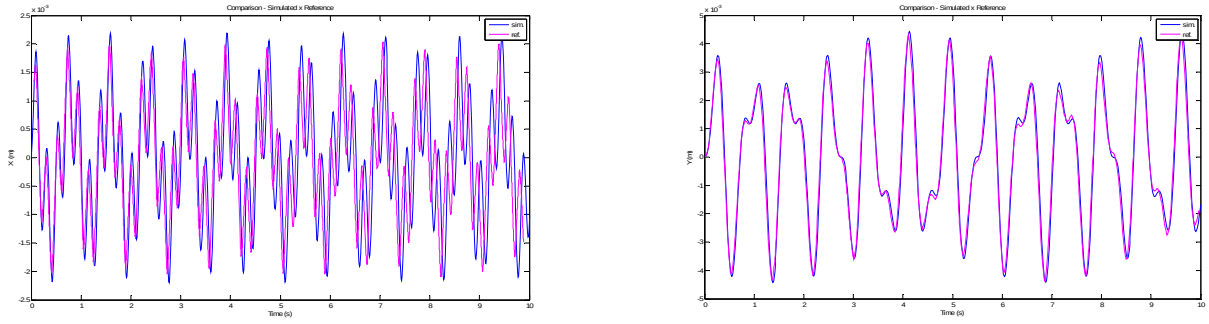


(a) (b)

Figure 4. Confrontation of the implemented methodology
(a): displacements in *x* direction; (b): displacements in *y* direction.

In order to test the mesh convergence of the discretization, the structure has been modeled using different numbers of elements *ne*, all with the same size. Figure 5 shows the displacement at the free extremity of the beam, obtained by using 1, 2, 3 and 10 elements.

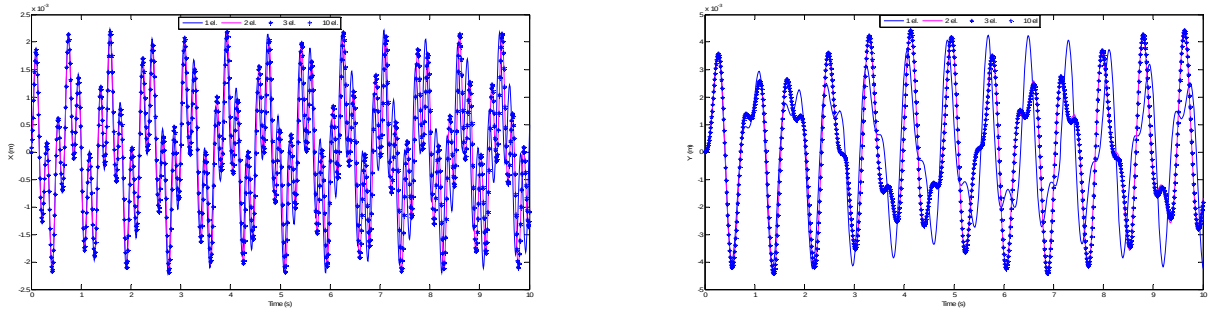


(a) (b)

Figure 5. Displacement in the x and y directions of the edge of the element using different numbers of elements.

It can be noticed that the difference between the responses obtained with the models using 2 and 10 elements is negligible. Thus the structure can be modeled using only 2 elements and 12 degrees-of-freedom without any decrease in accuracy. When the structure is modeled with a minimum number of elements, it may be necessary to use the shape functions to reconstruct the displacement fields inside the elements, as combinations of the nodal displacements and rotations. The accuracy of such procedure was evaluated by discretizing the beam with 2 and 10 elements and comparing the displacement responses at the point $s$=0.24 m, which coincides with a node of the 10-element model but does not so coincide with a node of the 2-element model. In Figure 6, the displacement responses are compared, showing that they are very close to each other. This fact confirms that, making the choice for discretization with few elements, the accuracy of the responses is maintained for any point along the beam length.

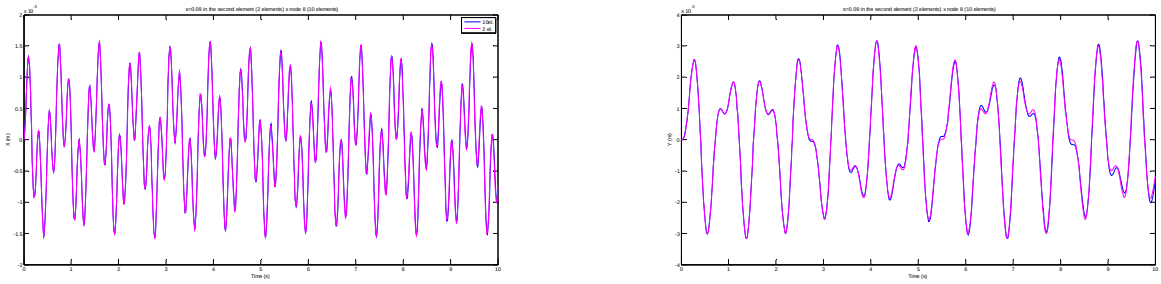

(a) (b)

Figure 6. Displacement inside the element using different number of elements
(a): displacements in *x* direction; (b): displacements in *y* direction.

### 3.2 Modeling of a riser

This section will present the results obtained from the dynamic analysis of a structure whose geometry is close to that a real riser used in the oil industry. This is a preliminary step towards the modeling of VIV accounting for fluid-structure interaction, using tridimensional CFD methods. Revolute joints are adopted in displacements both the extremities and the torsional degrees-of-freedom were eliminated, allowing rotation in the directions *x* and *y*, as shown in Figure 7. The structural properties are given in Table 1.

It is important to note that to obtain larger displacements (and geometrically nonlinear, consequently) we used an elasticity modulus lower than that used in real risers. This procedure aims to test the stability of the numerical integration method, as it is known that the more pronounced the nonlinear behavior, the greater the difficulty of convergence.

In these first tests, the structure is assumed to be excited by non-conservative, time-dependent hydrodynamic forces which are modeled by the semi-empirical Morison equations, using normal and transverse drag coefficients obtained from the literature (Santos, 2007). According to these equations, the normal and tangential drag forces are given, respectively, by:

$$\mathbf{f}_{an} = \frac{1}{2}\rho_f D_r C_{an} \mathbf{v}_{rn} \left|\mathbf{v}_{rn}\right| \tag{35}$$

$$\mathbf{f}_{at} = \frac{1}{2}\rho_f D_r C_{at} \mathbf{v}_{rt} \left|\mathbf{v}_{rt}\right| \tag{36}$$

where $\mathbf{v}_r$ is the relative velocity of the fluid, given by the expression $\mathbf{v}_r = \mathbf{v}_f - \mathbf{v}_c$, where $\mathbf{v}_f$ is the velocity of the fluid and $\mathbf{v}_c$ is the velocity of the cylinder. Hence, $\mathbf{v}_{rn}$ and $\mathbf{v}_{rt}$ are, respectively, the normal and the transversal component of $\mathbf{v}_r$; $\rho_f$ is the density of the fluid and $D_r$ is the diameter of the cable.

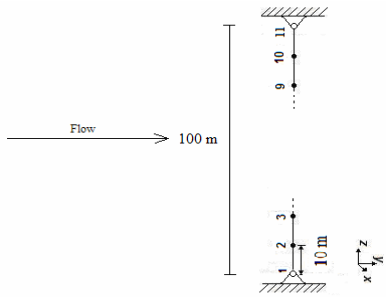


Figure 7. Layout of the structural model simulated.

Table 1. Properties of the modeled structure.

| Properties | Young's Module | Poisson Ration | Internal Radius (Ri) | External Radius (Re) | Cross Sectional Area | $C_{at}$ | $C_{an}$ | $V_f$ | Density |
|---|---|---|---|---|---|---|---|---|---|
| Values | 2.08e8 N/m² | 0.3 | 0.1800 m | 0.2000 m | 0.0239 m² | 0.05 | 0.6 | 0.8 m/s | 3.0e3 Kg/m³ |

Note that despite the structural model is represented by a line (2D), the methodology includes the tri-dimension modeling, and in this simulation to simplify the model, was chosen an excitement on just one direction. Figure 8 shows the displacement obtained at the time $t$ = 10.66 seconds and the temporal response obtained at the node 6 and direction y.

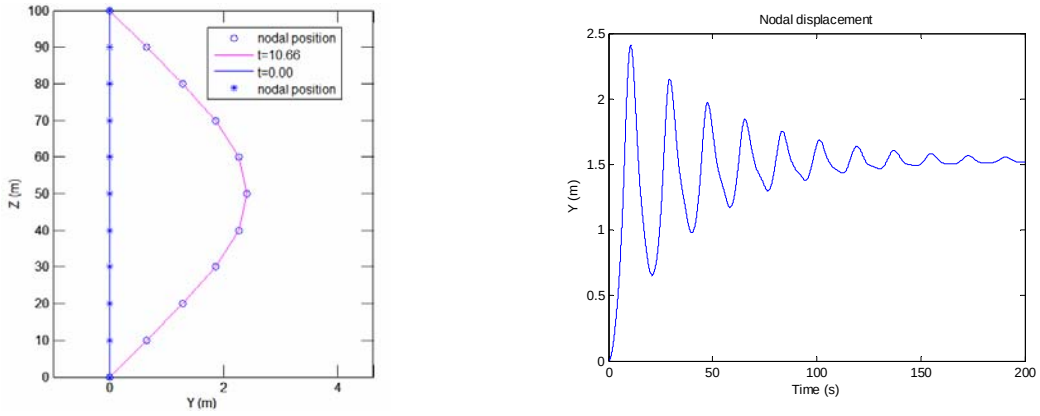


(a) (b)

Figure 8. Lateral displacement field and temporal response of the beam.

## 5. CONCLUSIONS

In this paper, the Cosserat beam theory has been implemented and from, upon comparison with the data found in literature, it was possible to assess and validate the implementation. This stage of validation was essential to evaluate the capability of the methodology, especially for the modeling of slender structures, such as risers used in the offshore industry. The numerical results demonstrate the possibility of characterizing accurately the nonlinear behavior with a reduced number of degrees-of-freedom. Clearly, the complexity of the formulation requires cumbersome algebraic manipulations, which must be tackled with the use of symbolic computations. Preliminary simulations were devoted to the characterization of VIV in offshore risers of large aspect rations, which is a very relevant industrial problem. Studies are being carried-out by the authors aiming at developing a numerical methodology for tridimensional fluid-structure interaction simulations based on the coupling of the structural model described in this paper with computational fluid dynamic procedures.

## 6. ACKNOWLEDGMENTS

The authors gratefully acknowledge the Brazilian Research Council – CNPq and Minas Gerais State Research Agency FAPEMIG for the continued support to their research work and funding through grants and scholarships.

## 7. REFERENCES

Alamo, F. J. C., Dinâmica de estruturas unidimensionais esbeltas utilizando o contínuo de Cosserat. Tese de doutorado, PUC-Rio 2006.
Antman S. S., 1995, “Nonlinear Problems of Elasticity", Applied Mathematical Sciences 107, New York: Springer-Verlag.
Bathe, K. J., 2007, “Conserving energy and momentum in nonlinear dynamics: a simple implicit time integration scheme”, Computers & Structures, vol. 85, no. 78, pp.437-445, 2007.
Cao, D. Q., Dongsheng, L., Charles, H., Wang, T., 2005, “Three dimensional nonlinear dynamics of slender structures”: Cosserat rod element approach. International Journal of Solids and Structures 43 (2006) 760-783.
Nayfeh, A. H., 1985, “Problems in Perturbation”. John Wiley Sons, Inc. (1985).
Pesce, C. P., 1997, “Mecânica de cabos e tubos submersos lançados em catenária: uma abordagem analítica e experimental”, Journal of Fluid Mechanics 116, 77 – 90.
Santos, L. R., 2007, “Moelling of the non linear dynamics of submarine cables”, thesis presented to COPPE/UFRJ.
Simo, J. C., 1985, “A finite strain beam formulation – the three-dimensional dynamic problem part I”. Computer Methods in Applied Mechanics and Engineering 49 55-70.
Vu-Quoc L., Simo, J. C., 1986, “A three-dimensional finite strain rod model part II: computational aspects”. Computer Methods in Applied Mechanics and Engineering 58 79-116.